Volume 59
Number 99
25 December 2023
Pages 14601–14728

ChemComm

Chemical Communications

rsc.li/chemcomm

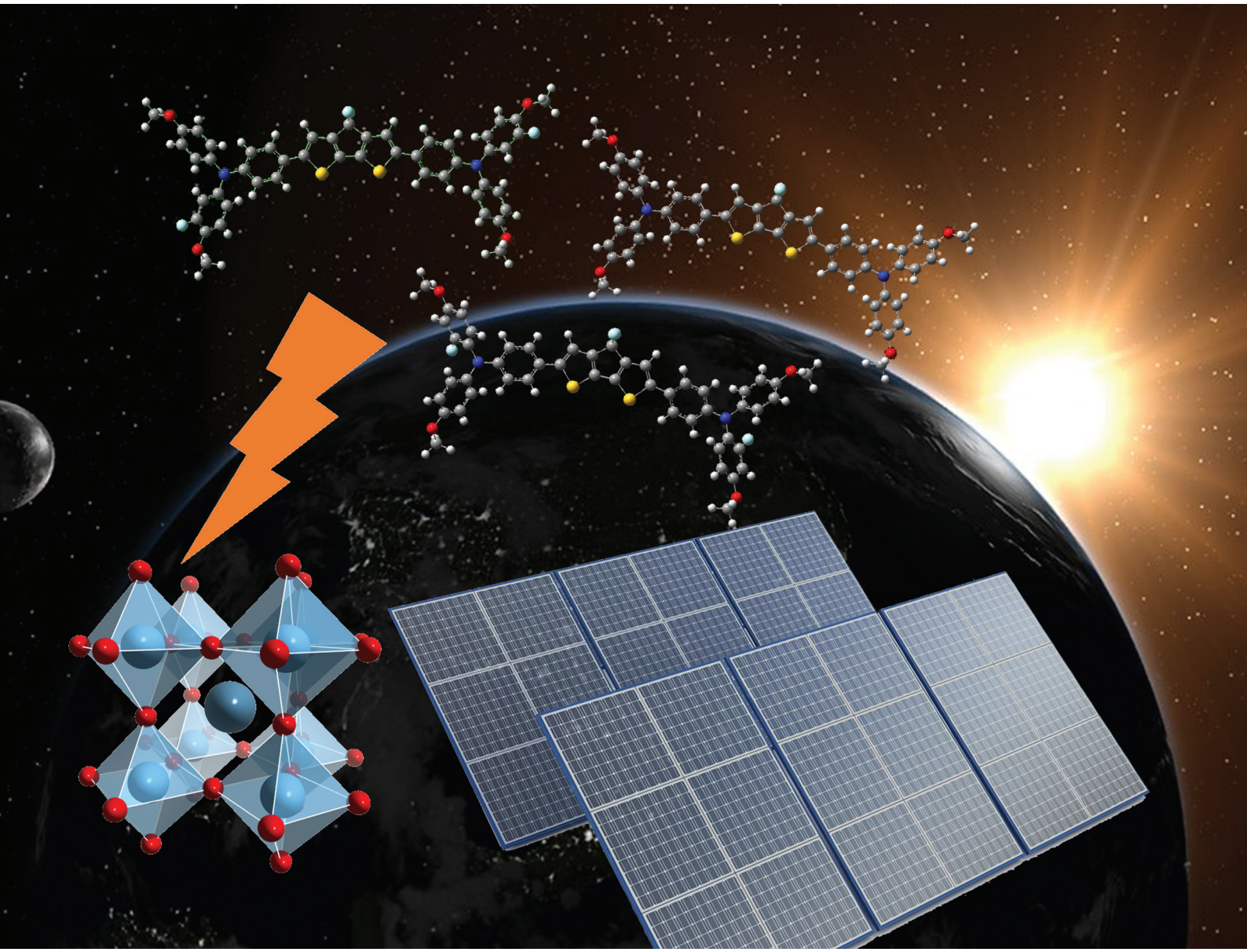

ISSN 1359-7345

ROYAL SOCIETY OF CHEMISTRY

COMMUNICATION

Kun-Mu Lee, Hsiao-Chi Hsieh, Shih-I Lu, Yan-Duo Lin *et al.*
Fluorination on cyclopentadithiophene-based hole-transport materials for high-performance perovskite solar cells

ChemComm

COMMUNICATION

Cite this: *Chem. Commun.*, 2023, **59**, 14653

Received 21st September 2023,
Accepted 9th November 2023

DOI: 10.1039/d3cc04699k

rsc.li/chemcomm

Fluorination on cyclopentadithiophene-based hole-transport materials for high-performance perovskite solar cells†

Gizachew Belay Adugna,‡[ab] Kun-Mu Lee,‡*[cdef] Hsiao-Chi Hsieh,*[g] Shih-I Lu,*[a] Yu-Chien Hsieh,[a] June Hung Yang,[a] Wei-Hao Chiu,[ce] Kang-Ling Liau,[h] Yu-Tai Tao[b] and Yan-Duo Lin*[a]

A new class of fluorinated cyclopenta[2,1-*b*:3,4-*b*′]dithiophene (CPDT)-based small molecules, namely YC-oF, YC-mF, and YC-H, are demonstrated as hole-transporting materials (HTMs) for high-performance perovskite solar cells (PSCs). PSCs employing YC-oF as the HTM delivered an excellent efficiency of 22.41% with encouraging long-term stability.

Organic–inorganic hybrid perovskite solar cells (PSCs) have attracted worldwide attention in the past few decades due to their excellent photovoltaic performance with their certified power conversion efficiency (PCE) skyrocketing from 3.8% to 26.1%.[1,2] To date, most efficient PSCs are based on an n–i–p device structure with 2,2′,7,7′-tetrakis-(*N*,*N*-di-p-methoxyphenylamine)-9,9′-spirobifluorene (spiro-OMeTAD) as the hole-transporting material (HTM), which plays a crucial role in the electron extraction and transport as well as the stability of PSCs.[3] Nonetheless, the shortcomings of spiro-OMeTAD are complicated synthesis and high purification costs, and the need for dopants, such as 4-*tert*-butylpyridine (*t*-BP) and lithium bis(trifluoromethanesulfonyl)imide (Li-TFSI), for improving the charge transport properties due to its intrinsic low hole mobility resulting from weak intermolecular interaction of the three-dimensional (3D) configuration.[4] Compared with spiro-type HTMs, the molecules with a planar core usually exhibit good π–π stacking and intermolecular interaction, leading to enhanced hole mobility and thus PCE.[5] Another promising strategy to increase hole mobility is to have a donor–acceptor–donor (D–A–D) conjugated backbone for the HTMs due to the intramolecular charge transfer (ICT) character, which may result in strong intermolecular interaction, thereby improving the charge-carrier transport.[6] Therefore, the development of the new two-dimensional HTMs with D–A–D structures giving improved photovoltaic performance is still urgently desirable.

Cyclopenta[2,1-*b*:3,4-*b*′]dithiophene (CPDT) derivatives have been widely employed as building blocks for highly efficient organic light-emitting diodes (OLEDs), organic field-effect transistors (OFETs), organic photovoltaic devices (OPVs), and dye-sensitized solar cells (DSSCs), due to their excellent charge-transport properties.[7–9] In recent years, our group developed a series of CPDT-based HTMs for application in PSCs and achieved excellent PCEs.[10–12] Recently, the introduction of the strong electronegativity of a fluorine atom into the organic conjugated molecule has been proven to be a successful strategy for enhancing photovoltaic properties and stability in PSCs because the fluorination can improve hole transport properties and enhance hydrophobicity.[12,13] However, to the best of our knowledge, the introduction of fluorine atoms into the CPDT backbone as HTMs for PSCs has never been explored.

Based on these considerations, in this work, we designed and synthesized three novel D–A–D HTMs, namely, **YC-oF**, **YC-mF**, and **YC-H**, which are composed of a difluoromethylene-bridged CPDT unit[14] as the conjugated skeleton featuring fluorinated and non-fluorinated triphenylamine (TPA) as the donor (Fig. 1). It is revealed that the fluorinated CPDT-based HTMs exhibited a higher hole mobility, well-matched energy alignment, better film morphology, and passivation effect. As a result, the PSCs using **YC-oF** as the HTM achieved a remarkable performance with a PCE of 22.41% and exhibited excellent operational stability. The synthetic route to the three HTMs is outlined in Scheme S1 (ESI†) and the detailed synthesis procedures and characterization data

[a] *Department of Chemistry, Soochow University, Taipei 11102, Taiwan. E-mail: ydlin@scu.edu.tw*
[b] *Institute of Chemistry, Academia Sinica, Taipei 115024, Taiwan*
[c] *Department of Chemical and Materials Engineering, Chang Gung University, Taoyuan 33302, Taiwan*
[d] *Division of Neonatology, Department of Pediatrics, Chang Gung Memorial Hospital, Linkou, Taoyuan 33305, Taiwan*
[e] *Center for Sustainability and Energy Technologies, Chang Gung University, Taoyuan 33302, Taiwan*
[f] *College of Environment and Resources, Ming Chi University of Technology, New Taipei City, 24301, Taiwan*
[g] *Department of Applied Materials Science and Technology, Minghsin University of Science and Technology, Hsinchu, Taiwan*
[h] *Department of Chemistry, National Central University, Taoyuan 32001, Taiwan*

† Electronic supplementary information (ESI) available. See DOI: https://doi.org/10.1039/d3cc04699k

‡ These authors contributed equally to this work.

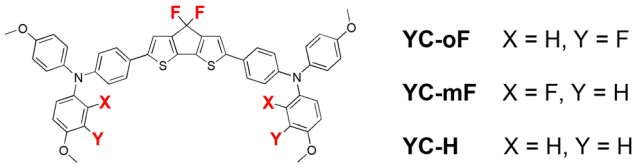

Fig. 1 Chemical structure of **YC** HTMs.

are provided in the ESI.† The synthesis costs of **YC-oF**, **YC-mF** and **YC-H** are calculated to be \$110.50 g^{-1}, \$111.10 g^{-1}, and \$75.64 g^{-1} (Tables S1–S13, ESI†), respectively, which are cheaper than that of spiro-OMeTAD (\$170–475 g^{-1}).[15] The normalized UV-vis absorption and photoluminescence spectra of **YC-oF**, **YC-mF** and **YC-H** in THF solution are shown in Fig. 2a. The absorption spectra of the three HTMs exhibit a featureless absorption band in the range from 400 to 550 nm with maximum absorption peaks at 463 nm for **YC-oF**, 459 nm for **YC-mF**, and 468 nm for **YC-H**, respectively. It may be attributable to the intramolecular charge transfer (ICT) transitions from the triphenylamine moieties to the central difluoromethylene-bridged CPDT, which is supported by time-dependent density functional theory (TDDFT) calculations shown in Fig. S13 and Tables S14–S16 (ESI†). The **YC-oF** and **YC-mF** show blue-shifted absorption peaks compared with that of **YC-H**, which may be attributed to the electron-withdrawing inductive effect of the fluorine atoms on the aromatic ring.[12,13] Moreover, the photoluminescence spectra of **YC-oF**, **YC-mF** and **YC-H** show intense emission in the region of 555–564 nm. The optical band

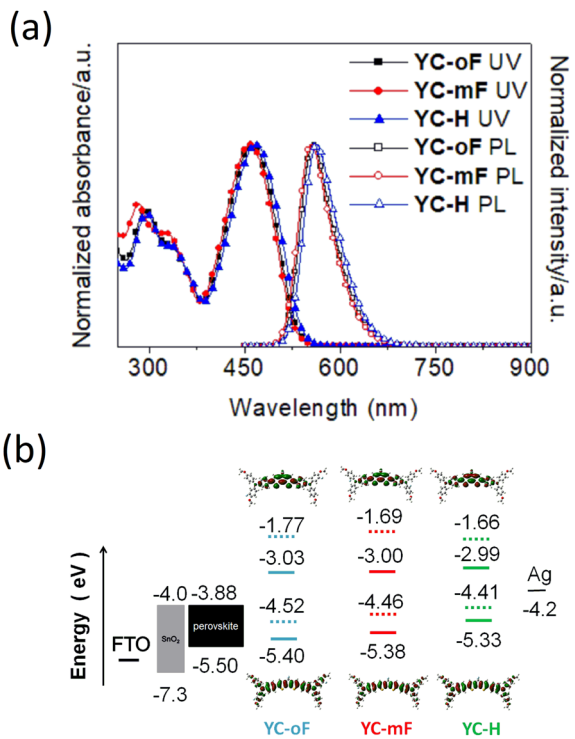

Fig. 2 (a) Normalized absorption and photoluminescence spectra of the **YC** series in THF solution. (b) The electron densities and energy level diagram of the **YC** series and related materials in a device. The calculated HOMO and LUMO values are presented as dashed lines.

gaps (E_g) of **YC-oF**, **YC-mF**, and **YC-H** were estimated to be 2.37, 2.38, and 2.34 eV, respectively, based on the intersection of normalized UV-vis and PL spectra. Thermogravimetric analysis (TGA) measurements (Fig. S14, ESI†) suggested that the **YC** series have good thermal stability (over 350 °C). However, the differential scanning calorimetry (DSC) measurements revealed that the glass transition temperature was not detected for the **YC** series of HTMs. As a result, the crystal properties of the **YC**-based HTMs were investigated by powder X-ray diffraction (PXRD). As shown in Fig. S15 (ESI†), the **YC** series showed crystalline morphology, suggesting that the enhanced π–π stacking could help HTMs to transport charge carriers efficiently.

Cyclic voltammetry (CV) and differential pulse voltammetry (DPV) (Fig. S16, ESI†) were performed to explore the electrochemical properties of the **YC** series. As depicted in Fig. 2b, the HOMO energy levels were calculated to be −5.40, −5.38, and −5.33 eV for **YC-oF**, **YC-mF** and **YC-H**, respectively. The corresponding LUMO energy levels are −3.03, −3.00, and −2.99 eV, respectively, according to the equation $E_{LUMO} = E_{HOMO} + E_g$. The energy levels of the **YC** series match well with those of the perovskites, indicating that the new HTMs should facilitate hole extraction and electron blocking from the perovskites to the metal electrodes. To shed light on the correlation between the molecular structures and electronic properties of the **YC** series, density functional theory (DFT) calculations at the B3LYP/6-31G(d,p) level were performed (Fig. 2b). It was found that the HOMO spreads over the difluoromethylene-bridged CPDT core with the peripheral arylamine groups, whereas the LUMO mainly locates on the difluoromethylene-bridged CPDT moiety. The HOMO and LUMO energy levels of **YC-oF**, **YC-mF** and **YC-H** were calculated to be −4.52/−1.77 eV, −4.46/−1.69 eV, and −4.41/−1.66 eV, respectively, with energy gaps of 2.75 eV, 2.77 eV, and 2.75, respectively (Fig. 2b). The calculated trends of the HOMO and LUMO energy levels are consistent with those of electrochemical data. The hole mobilities of the **YC** series and spiro-OMeTAD were determined according to the space-charge-limited-current (SCLC) method based on the hole-only devices with the structure of ITO/PEDOT:PSS/HTM/MoO_3/Ag (Fig. S17, ESI†). The hole mobilities of **YC-oF**, **YC-mF**, **YC-H** and spiro-OMeTAD were estimated to be 6.57×10^{-4}, 2.09×10^{-4}, 2.94×10^{-5} and 8.06×10^{-5} $cm^2\ V^{-1}\ s^{-1}$, respectively. The introduction of a fluorine atom onto the triphenylamine end-group of **YC-oF** and **YC-mF** increases the hole mobility, compared with **YC-H** without the fluorine atom on the TPA unit. This is probably attributable to the strengthened intermolecular packing because the fluorine substitution may result in larger dipole–dipole interactions among adjacent molecules. A similar phenomenon has been observed in our previous fluorinated HTMs.[12]

The steady-state photoluminescence (PL) and time-resolved photoluminescence (TRPL) data were measured to assess the charge dynamics between the HTMs and perovskites. As shown in Fig. S18 (ESI†), compared with the pristine perovskite film, the PL intensities of perovskite/**YC** series and perovskite/spiro-OMeTAD exhibit a significantly quenched intensity, which suggests an efficient hole transfer process at the interface of the perovskite layer/HTMs. Meanwhile, **YC-oF** showed the strongest PL quenching

capability with respect to other HTMs, indicating the fastest hole extraction process at the **YC-oF**/perovskite interface. As depicted in Fig. S18b (ESI†), the TRPL profiles of pristine perovskite films and HTMs/perovskites were fitted with the bi-exponential formula. The pristine perovskite film exhibits the longest average decay lifetime (104.9 ns). After deposition of the HTMs on the perovskite layer, a shortened average decay lifetime was observed. The average decay lifetimes of **YC-oF**/perovskite, **YC-mF**/perovskite, **YC-H**/perovskite, and spiro-OMeTAD/perovskite were calculated to be 9.91, 15.89, 35.47 and 33.51 ns, respectively. In particular, the **YC-oF**/perovskite shows the shortest average decay lifetime, indicating that the hole injection from the perovskite to **YC-oF** is more efficient than to other HTMs, which was consistent with the results of SCLC experiments.

To get insight into the interaction between perovskite films and the **YC** series, DFT calculations were employed to calculate the binding energies. As shown in Fig. S19 (ESI†) the binding energies between the perovskite and HTMs were −216.61, −209.28, and −188.40 kcal mol^{-1} for **YC-oF**, **YC-mF**, and **YC-H**, respectively, suggesting the tighter packing between **YC-oF** and the perovskite film, leading to more efficient hole extraction at the interface of the perovskite and **YC-oF**, and thus passivating the perovskite surface. X-ray photoelectron spectroscopy (XPS) was performed to explore the chemical interaction between the **YC**-based HTMs and the pristine perovskite (Fig. S20, ESI†). The peaks in the XPS spectra of Pb 4f and I 3d were observed to locate at 138.9, 143.7 eV and 619.7, 631.2 eV, respectively, for the pristine perovskite, which can be assigned to Pb $4f_{7/2}$, $4f_{5/2}$, I $3d_{5/2}$ and $3d_{3/2}$, respectively. The **YC**-capped perovskite films exhibited a shift of Pb 4f and I 3d peaks toward the lower binding energy. In addition, the pristine perovskite displayed two weak Pb 4f peaks at 137.2 and 142.1 eV, assigned to the signals of Pb^0. After coating HTMs on the perovskite, the Pb^0 peaks completely disappeared, suggesting efficient passivation of the perovskite surface. Moreover, S 2p peaks of **YC**-treated perovskite films shifted toward higher binding energies in comparison with pristine **YC**-based films. These results indicate that all the **YC**-based HTMs can interact with Pb^{2+}, which is beneficial to the interfacial passivation, and thus afford a better PSC.

The surface morphology and roughness of the pristine perovskite film with and without HTMs were investigated by scanning electron microscopy (SEM) and atomic force microscopy (AFM). As illustrated in Fig. S21 (ESI†), the top-view SEM images of the perovskite layers covered with **YC-oF**, **YC-mF**, and **YC-H** films exhibited compact and homogeneous surfaces with full surface coverage, which showed better charge transfer properties as well as hole mobilities and then enhanced J_{sc} and FF in PSCs. Furthermore, the AFM measurements showed that the root-mean-square (RMS) roughness values of the **YC-oF**, **YC-mF**, and **YC-H**-capped perovskite are 1.46, 1.54 and 1.55 nm, respectively (Fig. S21, ESI†), which are smaller than that of the pristine perovskite film (12.30 nm). Meanwhile, it was observed that **YC-oF** and **YC-mF**-based films showed slightly smoother and more uniform surfaces relative to **YC-H**-based films on the perovskite surface, which could not only improve the charge extraction and collection but also protect the perovskite layer from moisture and/or oxygen penetration.

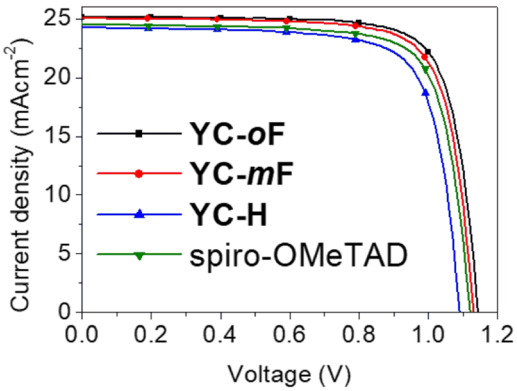

Fig. 3 *J*–*V* curves of devices at a reverse scan based on **YC** series and spiro-OMeTAD as HTMs.

To evaluate the photovoltaic performance of the **YC** series as potential HTMs, PSCs with an n–i–p device configuration of FTO/SnO_2/$Cs_{0.05}MA_{0.2}FA_{0.75}Pb(Br_{0.05}I_{0.95})_3$/HTMs/Ag were fabricated. Fig. 3 shows the photocurrent density–voltage (*J*–*V*) characteristics of the best devices employing **YC-oF**, **YC-mF**, **YC-H**, and spiro-OMeTAD in PSCs with the related parameters summarized in Table 1. The details of the device fabrication process can be found in the ESI.† Fig. S22 (ESI†) shows the cross-section SEM image of the device with **YC-oF** as the HTM. The film thicknesses of the perovskite layer and **YC-oF** are ~629 and 238 nm, respectively, with a dense film morphology of the perovskite and uniform HTM layer, which is favorable for charge extraction.

The **YC-H**-based devices exhibited a PCE of 20.36% with an open-circuit voltage (V_{oc}) of 1.10, a short-circuit density (J_{sc}) of 24.30 mA cm^{-2} and a fill factor (FF) of 76.18%, which were lower than those of the device with **YC-oF** (V_{oc} = 1.14 V, J_{sc} = 25.20 mA cm^{-2}, FF = 78.03%, and PCE = 22.41%) and **YC-mF** (V_{oc} = 1.13 V, J_{sc} = 25.06 mA cm^{-2}, FF = 76.95%, and PCE = 21.79%) for a reverse scan, along with negligible hysteresis (Fig. S23, ESI†). It seems that the incorporation of one fluorine atom on the methoxyphenyl groups of the **YC-oF** and **YC-mF** molecule is a successful approach for enhancing the PCE. The higher PCEs for **YC-oF**- and **YC-mF**-based devices could be attributed to the better hole mobility (Fig. S17, ESI†), strong hole-extraction capability (Fig. S18, ESI†), and lower HOMO energy level to decrease V_{oc} loss (Fig. 2b), all of which may facilitate the charge transport and thus improve PCEs. Moreover, the devices based on **YC-oF** and **YC-mF** show higher PCEs than the control spiro-OMeTAD-based device (21.04%). Furthermore, the PCEs of 20 devices were measured to evaluate the reproducibility using the **YC** series as HTMs. Fig. S24

Table 1 Device parameters of the champion PSCs based on **YC-oF**, **YC-mF**, **YC-H** and spiro-OMeTAD HTMs

HTM	Scan direction	V_{oc} [V]	J_{sc} [mA cm^{-2}]	FF (%)	PCE_{max} [%]
YC-oF	Reverse	1.14	25.20	78.03	22.41
YC-mF	Reverse	1.13	25.06	76.95	21.79
YC-H	Reverse	1.10	24.30	76.18	20.36
Spiro-OMeTAD	Reverse	1.12	24.52	76.63	21.04

(ESI†) shows a narrower distribution of the photovoltaic performance, and yields the average PCE values of 22.20%, 21.57%, and 20.21% for PSCs based on **YC-oF**, **YC-mF**, and **YC-H**, respectively, indicating their good reproducibility. To evaluate the photovoltaic performance of the **YC** series as dopant-free HTMs in PSCs, the PSC devices without dopants were fabricated. As shown in Fig. S25 and Table S18 (ESI†), the **YC-oF**, **YC-mF**, and **YC-H**-based devices showed low efficiency values, which reached the PCEs of 13.48, 12.12, and 10.63%, respectively, under a reverse scan.

The incident photo-to-electron conversion efficiency (IPCE) spectra of the devices are shown for each HTM in Fig. S26 (ESI†). The integrated photocurrents from the IPCE spectra were 25.02, 24.88, 24.11 and 24.37 mA cm^{-2} for the **YC-oF**-, **YC-mF**-, **YC-H**-, and spiro-OMeTAD-based PSCs, respectively, consistent with the J_{sc} values from the *J–V* curves. To further verify the PCEs of the PSCs based on the **YC** series as HTMs, the steady-state efficiencies as a function of time at the maximum power point (MPP) were evaluated, which show a highly stable PCE of 22.27%, 21.61%, and 20.28% after 200 s duration for **YC-oF**, **YC-mF**, and **YC-H**, respectively (Fig. S27, ESI†).

The long-term stability of PSC devices containing the **YC** series and spiro-OMeTAD without encapsulation was examined at room temperature with 40% humidity and the thermal stability monitored at 85 °C in a glove box under dark storage. As depicted in Fig. S28a (ESI†), the new fluorinated **YC** HTMs show promising stability and retained over 88% of their initial efficiency after 1000 h. In contrast, the device based on spiro-OMeTAD preserved 73% of the original value. As shown in Fig. S29 (ESI†), the water-contact angles on **YC-oF** (135°), **YC-mF** (124°), and **YC-H** films (115°) are much higher than that on spiro-OMeTAD film (73°), indicating that the fluorinated HTMs can effectively prevent moisture from penetrating into the perovskite film, and thus exhibited a higher stability of the device. A thermal stability test of the devices was also conducted, and the results are shown in Fig. S28b (ESI†). Devices based on **YC-oF**, **YC-mF**, and **YC-H** conserved 86%, 82%, and 78%, respectively, of the initial PCE after 600 h. In comparison, a more significant degradation was observed for the device with spiro-OMeTAD (61%). Moreover, when subjected to continuous light soaking at 1 sun illumination, it was found that the **YC** series-based cells retained over 70% of the original efficiency after 800 h, while the spiro-OMeTAD-based PSCs exhibited the poorest stability, with only 57% of the initial efficiency maintained (Fig. S28c, ESI†). Therefore, it is demonstrated that the hydrophobic nature of new fluorinated HTMs is favorable to the device stability.

In summary, three novel D–A–D type HTMs, namely **YC-oF**, **YC-mF**, and **YC-H**, with a difluoromethylene-bridged CPDT core have been facilely synthesized at a low cost. The best PSC with **YC-oF** showed an excellent PCE of 22.41%, along with negligible hysteresis. The decent efficiency could be mainly attributed to the improved energy level alignment, hole-drift mobilities, and smoother film morphology, leading to an efficient hole extraction process. Furthermore, the **YC**-based devices exhibited excellent long-term stability owing to the good hydrophobic characteristics. These results demonstrated that a F-substituted molecular design strategy is an effective route for the development of high-performance HTMs for efficient and stable PSCs.

Y.-D. Lin thanks the support from the Ministry of Science and Technology, Taiwan (Grant Number MOST 111-2628-M-031-001-MY3). K.-M. Lee thanks the support from the Ministry of Science and Technology, Taiwan (Grant Number MOST 111-2223-E-182-001-MY4), Chang Gung University (QZRPD181) and Chang Gung Memorial Hospital, Linkou, Taiwan (CMRPD2M0042). We are grateful to the National Center for High-performance Computing for computer time and facilities.

Conflicts of interest

There are no conflicts to declare.

Notes and references

1 A. Kojima, K. Teshima, Y. Shirai and T. Miyasaka, *J. Am. Chem. Soc.*, 2009, **131**, 6050–6051.
2 NREL, Best *Research-Cell Efficiency Chart*, **https://www.nrel.gov/pv/cell-efficiency.html** (accessed: 2023).
3 H. Min, D. Y. Lee, J. Kim, G. Kim, K. S. Lee, J. Kim, M. J. Paik, Y. K. Kim, K. S. Kim, M. G. Kim, T. J. Shin and S. Il Seok, *Nature*, 2021, **598**, 444–450.
4 J. Wang, H. Zhang, B. Wu, Z. Wang, Z. Sun, S. Xue, Y. Wu, A. Hagfeldt and M. Liang, *Angew. Chem., Int. Ed.*, 2019, **58**, 15721–15725.
5 H. Guo, H. Zhang, C. Shen, D. Zhang, S. Liu, Y. Wu and W.-H. Zhu, *Angew. Chem., Int. Ed.*, 2021, **60**, 2674–2679.
6 X. Yin, Z. Song, Z. Li and W. Tang, *Energy Environ. Sci.*, 2020, **13**, 4057–4086.
7 R. P. Ortiz, A. Facchetti, T. J. Marks, J. Casado, M. Z. Zgierski, M. Kozaki, V. Hernández and J. T. L. Navarrete, *Adv. Funct. Mater.*, 2009, **19**, 386–394.
8 M. Zhang, Y. Wang, M. Xu, W. Ma, R. Li and P. Wang, *Energy Environ. Sci.*, 2013, **6**, 2944–2949.
9 J. Huang, S. Li, J. Qin, L. Xu, X. Zhu and L.-M. Yang, *ACS Appl. Mater. Interfaces*, 2021, **13**, 45806–45814.
10 K.-M. Lee, W.-H. Chiu, Y.-H. Tsai, C.-S. Wang, Y. T. Tao and Y.-D. Lin, *Chem. Eng. J.*, 2022, **407**, 131609.
11 K.-M. Lee, S. Y. Abate, J. H. Yang, W.-H. Chiu, S. Ahn, S.-R. Li, K.-L. Liau, Y. T. Tao and Y.-D. Lin, *Chem. Eng. J.*, 2023, **454**, 139926.
12 K.-M. Lee, Y.-S. Huang, W.-H. Chiu, Y.-K. Huang, G. Chen, G. B. Adugna, S.-R. Li, F.-J. Lin, S.-I. Lu, H.-C. Hsieh, K.-L. Liau, C.-C. Huang, Y. Tai, Y. T. Tao and Y.-D. Lin, *Adv. Funct. Mater.*, 2023, 2306367.
13 Z. Li, Y. Tong, J. Ren, Q. Sun, Y. Tian, Y. Cui, H. Wang, Y. Hao and C.-S. Lee, *Chem. Eng. J.*, 2020, **402**, 125923.
14 Y. Le, M. Nitani, M. Ishikawa, K.-I. Nakayama, H. Tada, T. Kaneda and Y. Aso, *Org. Lett.*, 2007, **9**, 2115–2118.
15 H. D. Pham, T. T. Do, J. Kim, C. Charbonneau, S. Manzhos, K. Feron, W. C. Tsoi, J. R. Durrant, S. M. Jain and P. Sonar, *Adv. Energy Mater.*, 2018, **8**, 1703007.

